BIOCHEMISTRY
including biophysical chemistry & molecular biology

Article

pubs.acs.org/biochemistry

Structural and Functional Characterization of Methicillin-Resistant *Staphylococcus aureus's* Class IIb Fructose 1,6-Bisphosphate Aldolase

Glenn C. Capodagli,[†] Stephen A. Lee,[†] Kyle J. Boehm,[†] Kristin M. Brady,[†] and Scott D. Pegan*[,‡]

[†]Department of Chemistry and Biochemistry, University of Denver, Denver, Colorado 80208, United States

[‡]Department of Pharmaceutical and Biomedical Sciences, University of Georgia, Athens, Georgia 30602, United States

ABSTRACT: *Staphylococcus aureus* is one of the most common nosocomial sources of soft-tissue and skin infections and has more recently become prevalent in the community setting as well. Since the use of penicillins to combat *S. aureus* infections in the 1940s, the bacterium has been notorious for developing resistances to antibiotics, such as methicillin-resistant *Staphylococcus aureus* (MRSA). With the persistence of MRSA as well as many other drug resistant bacteria and parasites, there is a growing need to focus on new pharmacological targets. Recently, class II fructose 1,6-bisphosphate aldolases (FBAs) have garnered attention to fill this role. Regrettably, scarce biochemical data and no structural data are currently available for the class II FBA found in MRSA (SaFBA). With the recent finding of a flexible active site zinc-binding loop (Z-Loop) in class IIa FBAs and its potential for broad spectrum class II FBA inhibition, the lack of information regarding this feature of class IIb FBAs, such as SaFBA, has been limiting for further Z-loop inhibitor development. Therefore, we elucidated the crystal structure of SaFBA to 2.1 Å allowing for a more direct structural analysis of SaFBA. Furthermore, we determined the K_M for one of SaFBA's substrates, fructose 1,6-bisphosphate, as well as performed mode of inhibition studies for an inhibitor that takes advantage of the Z-loop's flexibility. Together the data offers insight into a class IIb FBA from a pervasively drug resistant bacterium and a comparison of Z-loops and other features between the different subtypes of class II FBAs.

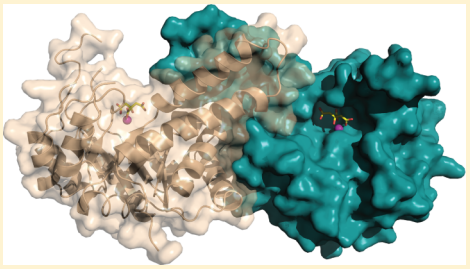

Staphylococcus aureus (*S. aureus*) is a Gram-positive bacterium responsible for what is commonly referred to as a staph infection. Symptoms of staph infections range from skin and soft tissue infection to necrotizing fasciitis, pneumonia, and even death.[1] Although staph infections are predominantly transmitted nosocomially, *S. aureus* has also been found in cases outside of a hospital setting.[2−6] In 2011, there were over 80,000 cases resulting in more than 11,000 deaths reported in the US caused by various strains of *S. aureus*.[3] Even with several advances having been made in combatting *S. aureus* infections in the form of various antibiotics, the bacterium has continued to survive and develop resistances.[7−13]

Infections by *S. aureus* were initially treated using penicillin starting in the 1940s; however, within a few years resistance to the treatment had emerged.[1] To combat this resistance, a penicillin analogue known as methicillin was created. Methicillin was first utilized to treat staph infections in 1959 and worked in the same manner as other penicillins by disrupting the class of proteins known as penicillin-binding proteins (PBPs), transpeptidase enzymes involved with cross-linking bacteria cell wall precursors.[1] Disruption of PBPs leads to weakened cell walls and eventually cell death. Yet, by the 1960s cases of methicillin-resistant *Staphylococcus aureus* (MRSA) strains began to emerge in Europe and the US.[14] Currently there are strains of MRSA resistant to all β-lactams including penicillin derivatives and cephalospoins, as well as other non-β-lactam antibiotics such as aminoglycosides like vanomycin, fluoroquinolones, and macrolides.[7−13]

MRSA was first thought to only occur in a hospital setting under conditions that increased the risk factor for exposure.[6] However, in the 1980s there were several outbreaks of MRSA in patients who had not encountered a hospital setting. Furthermore, in 1999 the Centers for Disease Control (CDC) reported on four previously healthy children whose skin infections were treated with cephalosporins, but whose eventual death was proven to be caused by MRSA.[5] As such MRSA is typically categorized into three main categories: Hospital-Acquired (HA), Healthcare-Associated Community-Onset (HACO), and Community-Acquired (CA). Although the number of MRSA cases reported has been on the decline, there were over 80,000 cases reported in the US in 2011, greater than 75% of which were either HA- or HACO-MRSA.[2−4] Interestingly, from 2005 to 2011 the incident rates of HA-MRSA and HACO-MRSA has declined by ∼54% and ∼27%, respectively, but CA-MRSA rates have only dropped by ∼5%.[4] The CDC estimates that roughly one-third of people carry some variant of *S. aureus* in their nose and that nearly one in 50 people carry MRSA without any symptoms.[3]

With the persistence and evolving nature of MRSA, increasing focus has been placed on potentially new pharmacological targets. One such target is *S. aureus's* fructose-1,6-bisphosphate aldolase (SaFBA). As a class II

Received: September 10, 2014
Revised: November 10, 2014
Published: November 12, 2014

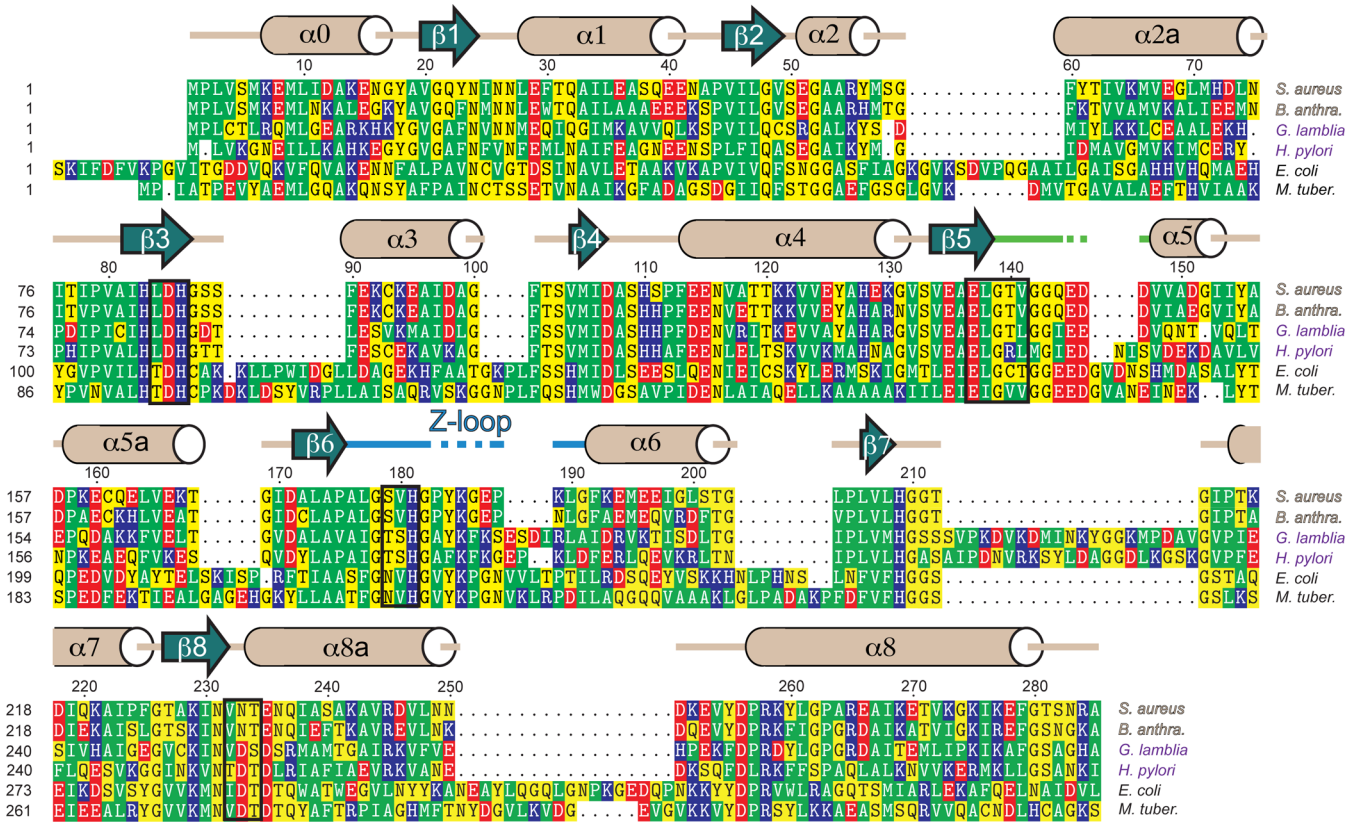

Figure 1. Sequence alignment of class II FBAs. FBAs are from *Staphylococcus aureus* (*S. aureus*; Q5HE75), *Bacillus anthracis* (*B. anthra*; PDB entry 3Q94_A), *Giardia lamblia* (*G. lamblia*; 3GAK_B), *Helicobacter pylori* (*H. pylori*; 3N9S_A), *Mycobacterium tuberculosis* (*M. tuber*; NP_334786), and *Escherichia coli* (*E. coli*; PDB entry 1DOS_A). FBA names are colored based on class II grouping: tan denotes class IIb-i, purple denotes class IIb-iv, and black denotes class IIa. Secondary structure of SaFBA according to Defined Secondary Structure of Proteins (DSSP) is shown as tan cylinders (helical regions), teal arrows (β-sheets), and tan lines (loops). Hashed lines represent residues for which electron density was not defined in the crystal structure. Green line represents the active site loop. Cyan line represents the Z-loop. Breaks denote regions were SaFBA does not have residues. Black brackets indicate residues that are part of SaFBA's active site. Amino acids are color-coded with respect to being acidic (red), basic (blue), polar uncharged (yellow), and hydrophobic nonpolar (green).

fructose 1,6-bisphosphate aldolase, SaFBA falls into one of two classes of fructose 1,6-bisphosphate aldolases (FBAs). Both class I and class II FBAs catalyze the reversible aldol condensation of dihydroxyacetone phosphate (DHAP) with glyceraldehyde 3-phosphate (G3P) to form fructose 1,6-bisphosphate (FBP).[15] However, the two enzyme classes differ in their mechanism of catalysis and prevalence among species. Specifically, class I FBAs utilize a lysine residue to generate a nucleophilic enamine from DHAP, whereas class II aldolases utilize a Zn(II) cation to stabilize the DHAP enolate intermediate involved in the aldol condensation reaction. Also, the location of a key amino acid side chain responsible for proton extraction and addition significantly differs.[16−18] Beyond the differences in their reaction mechanisms, the two classes of FBAs distinctly differ in their distribution among species. Higher organisms such as humans possess only class I FBAs, whereas protozoa, bacteria, fungi, and blue-green algae primarily have class II FBAs, with a few possessing both.[19−21]

Class II FBAs are essential for the survival of both Gram-positive and Gram-negative bacteria as shown through knockout studies of several organisms including *Mycobacterium tuberculosis, Escherichia coli, Streptomyces galbus, Bacillus subtilis, Peudomonas aeruginosa, Streptococcus pneumonia, and Candida albicans* in which deletion of the *fba* gene resulted in a loss of viability.[22−31] Even in organisms that possess both class I and class II FBAs, such as *E. coli,* the lack of the class II FBA was shown to be detrimental.[23,32,33] As a result, significant efforts have been taken to develop inhibitors of class II FBAs for use as treatments related to bacterial and protozoan infections such as tuberculosis.[34−38] Therefore, selective inhibitors developed for class II FBAs are unlikely to generate toxic effects through disruption of the human class I FBA thus making class II FBAs a highly sought after bacterial target for pharmacological development.

Class II FBAs can be categorized as class IIa or class IIb on the basis of sequence homology. Although class IIa FBAs were traditionally thought to be all dimers, recent findings have shown that there exist certain exceptions, such as the class IIa FBA from *Mycobacterium tuberculosis* (MtFBA), which forms a tetramer.[17] Meanwhile, class IIb FBAs can range from dimers to tetramers to even octomers and tend to be shorter in amino acid length than their class IIa counterparts.[17,19,20,39,40] Furthermore, sequence alignments of class IIb FBAs suggest that this group might be divided into at least four additional subtypes (i-iv) although certain discrepancies exist within the purely sequence-based categorization.[40,41] To date, only the structures of class IIb-i FBAs have been studied in regard to their enzymatic capacities.[20,42−45] Based on sequence composition, SaFBA appears to belong to the class IIb-iv of FBAs; however, no structure of either SaFBA, or a proposed class IIb-iv FBA, has yet been reported (Figure 1).

dx.doi.org/10.1021/bi501141t | *Biochemistry* 2014, 53, 7604−7614

This lack of information has proven problematic in light of the discovery that 8-hydroxyquinoline-2-carboxylic acid (HCA) inhibits MtFBA, a class IIa FBA. Unlike previous class II FBA inhibitors whose design has centered primarily on developing analogues of DHAP and FBP to act as competitive active site inhibitors, HCA capitalizes on the flexibility of an active site zinc-binding loop (Z-loop) found within MtFBA to act as a noncompetitive inhibitor.[46] This mode of inhibition appears to side step previous issues of class I FBA promiscuity of the substrate mimic-styled inhibitors, plus the need for inhibitors to possess highly charged phosphate groups, which hinder membrane permeability.[19,34−37,43,47−49] Regrettably, the composition of the Z-loop region as well as other potential structural features in the vicinity appear to differ between the two subclasses of FBAs and even among class IIb FBA subtypes (Figure 1).

To gain a more complete understanding of how SaFBA compares to its class II FBA counterparts, the first X-ray crystal structure of SaFBA was elucidated to 2.1 Å and compared to that of MtFBA as well as to other class IIb FBAs. Analysis of the crystal structure was performed revealing that the Z-loop in SaFBA can be readily displaced from the active site. Furthermore, the K_M value for one of the SaFBA substrates, FBP, as well as the K_i for HCA were determined and compared to those of MtFBA.

EXPERIMENTAL PROCEDURES

Materials. Chemicals, biochemicals, buffers, and solvents were purchased from Sigma-Aldrich Chemical Co. (St. Louis, MO), Fisher Scientific, Inc. (Pittsburgh, PA), Acros Organic (Morris Plains, NJ), or Worthington Biochemical Corp, (Lakewood, NJ) unless otherwise indicated. Enzymatic assay reagents, including bovine serum albumin (BSA, catalog no. A3059-50G), nicotinamide adenine dinucleotide hydrate (NAD^+, catalog no. 43407-25G), rabbit glyceraldehyde 3-phosphate dehydrogenase (GAPDH, catalog no. G2267-10KU), and D-fructose 1,6-bisphosphate tetra-(cyclohexammonium) salt (FBP, catalog no. F0752-5G), were purchased from Sigma-Aldrich. Resazurin sodium salt (catalog no. 189900250) and 8-hydroxyquinoline-2-carboxylic acid (HCA, catalog no. 347620010) were obtained from Acros Organics. Diaphorase was purchased from Worthington (catalog no. 4327). The Amicon Ultra-15 centrifugal filter devices were obtained from Millipore (UFC901024). The Ni-NTA and the Superdex-S200 High Resolution resins were obtained from Qiagen (Valencia, CA) and GE Healthcare, respectively. Costar 96-well half area, black flat-bottom polystyrene plates were purchased from Corning (catalog no. 3694).

Production and Purification of SaFBA. The production of the FBA expression vector for a methicillin-resistant strain of *Staphylococcus aureus* (SaFBA) was generated using *Escherichia coli* (*E. coli*) BL21 optimized synthesis by Genscript, Inc. The SaFBA expression construct encodes the 289 amino acids from UniProtKB entry Q5HE75.1 as well as six histidines and a stop codon to generate a C-terminal histidine tag. The pET11a-*fbaA* plasmid was introduced into *E. coli* BL21 (DE3) by heat-shock transformation for enzyme expression. The resulting plasmid was then purified, restriction analyzed, and sequenced to verify the construct. The expression system produced a C-terminal, His-tagged fusion protein, which is herein termed SaFBA. Cells containing SaFBA were grown in 12 L of LB broth containing 100 μg/mL ampicillin until an OD_{600} of 0.6 was reached. Expression of the SaFBA was induced by addition of IPTG to a final concentration of 0.4 mM, and the culture was grown for an addition 4−6 h at 25 °C. Following this period, the bacterial cells were isolated via centrifugation at 3,000 × *g* for 10 min and stored at −80 °C. The cell pellets were suspended in Buffer A [300 mM NaCl and 50 mM Tris (pH 8.0)] and lysed by addition of 5 mg of chicken lysozyme followed by sonication. The insoluble cell debris was separated via centrifugation for 45 min at 17,000 × *g*. SaFBA was purified from the resulting supernatant by using a Qiagen Ni-NTA column and eluted with Buffer A containing 300 mM imidazole followed by buffer exchange into Buffer B [100 mM NaCl, 20 mM Tricine (pH 8.0), 2 mM DTT, and 0.1 mM $ZnCl_2$] by passage over a Superdex-S200 High Resolution column. The purified SaFBA was concentrated to 12 mg/mL via 10,000 molecular weight cutoff centrifugal filter units (Millipore Cork, IRL) at 4000 × *g*. The final protein was then filtered through 0.22 μM Costar spin filters. All protein concentrations were determined through UV−visible spectroscopy at 280 nm using molar extinction coefficients experimentally derived by the method of Gill and von Hippel.[50]

FBA Enzymatic FBP Cleavage Assays. The activity of FBAs was monitored through a fluorescence-based assay measuring the increase in fluorescence due to conversion of resazurin to resorufin via diaphorase when coupled with the oxidation of NADH to NAD^+. The assay mixture (final volume of 50 μL) contained 0.4 mM NAD^+, 8 units/mL GAPDH, 0.01% (w/v) BSA, 2 mM DTT, 15 mM NaH_2AsO_4, 100 mM Tris HCl (pH 7.8), 100 mM CH_3COOK, 180 nM MtTPI, 1 unit/μL diaphorase, and 50 μM resazurin. A final assay concentration of 40 nM SaFBA was used. All assays were performed at room temperature and in duplicate using Costar 96-well half area, black flat-bottom polystyrene plates (Corning). All FBA activity assays were conducted using a TECAN M1000 plate reader by measuring the fluorescence of resorufin at 585 nm when it was excited at 535 nm. A standard curve for FBP conversion was determined previously for the conversion to molecules turned over.[46] The values for K_M and k_{cat} were determined from the rates of the initial velocity data as the concentration of FBP was varied from 0 μM to 4000 μM for the Michaelis−Menten equation, $\nu = V_{max}/(1 + K_M/[S])$, using the Enzyme Kinetics Module of SigmaPlot, version 12.2 (SPSS, Inc.).

The IC_{50} value for the inhibition of SaFBA by HCA was determined at HCA concentrations ranging from 0 to 2 mM, with the FBP concentration held constant at 250 μM. The percent inhibition (I%) was calculated using the formula $I\% = [1 - (\nu_{sample} - \nu_{negative\ control})/(\nu_{positive\ control} - \nu_{negative\ control})] \times 100$. The resulting I% values were fit via nonlinear regression to the equation $I\% = I\%_{max}/(1 + IC_{50}/[HCA])$ using the Enzyme Kinetics Module of SigmaPlot. The IC_{50} value for citrate inhibition of SaFBA was conducted in a similar manner with the exception that sodium citrate at a pH = 7.8 was utilized and its concentration was varied from 0 mM to 140 mM.

To determine the mode of action of HCA, inhibition studies were conducted using HCA concentrations ranging from 0 to 500 μM with three additional concentrations of FBP ranging from 125 to 1,000 μM used to initiate the reaction. Initial velocity data were fit using nonlinear regression analysis to each of the equations describing partial and full models of competitive, uncompetitive, noncompetitive, and mixed inhibition using the Enzyme Kinetics Module of SigmaPlot. On the basis of the analysis of fits through "goodness-of-fit" statistics,

the full mixed inhibition model was determined with the equation $\nu = V_{max}/[((K_M/[S]) \times (1 + [I]/K_i) + (1 + [I]/(\alpha \times K_i))]$, where [S] = [FBP], [I] = [HCA], and K_i is the constant for dissociation of HCA from free SaFBA.

Crystallization of SaFBA. The initial crystal conditions for SaFBA were determined through high-throughput screening of Qiagen Classics I and II screens in a 96-well sitting drop format using an Art Robbins Phoenix robot. Drops contained 0.4 μL of precipitate with a 100-μL reservoir volume. Initial screening resulted in crystals from conditions with 1.8 M ammonium citrate (pH 7.0) and 12 mg/mL of SaFBA; however, further screening containing 1.6 M ammonium citrate (pH 7.5) produced the most viable crystals. These crystals were optimized using the Additive HT Screen from Hampton Research. Final SaFBA crystals were obtained through hanging-drop vapor diffusion at 20 °C and included using a 500-μL reservoir of 1.6 M ammonium citrate (pH 7.5) with 4-μL hanging drops mixed 1:1 with protein solution and an additional 0.25 μL of 3 M dimethylethylammonium propanesulfonate, a zwitterionic nondetergent sulfobetaine termed NSDB-195.

X-ray Structure of SaFBA. An X-ray data set was collected using a crystal mounted onto a nylon loop flash-cooled in liquid nitrogen. The crystal was mounted under a stream of dry N_2 at 100 K. An SaFBA data set with resolution to 2.10 Å was collected at Advance Light Source (ALS) beamline 4.2.2 using a monochromatic X-ray beam of 1.00 Å with a CMOS_8 M detector. X-ray images were indexed, processed, integrated, and scaled using XDS.[51] An initial phase solution was elucidated using holo-MtFBA [Protein Data Bank (PDB): 4DEF] as a starting model for molecular replacement using Phaser.[52] The structure was refined using iterative cycles of model building and refinement using COOT and phenix.refine, respectively.[53,54] Water molecules were added to $2F_o-F_c$ density peaks of >1σ using the Find Water COOT program function. The final model was checked for structural quality using the CCP4 suite programs Procheck and Sfcheck. The data refinement statistics are listed in Table 1.

Table 1

	SaFBA
Data Collection	
space group	$P2_12_12$
unit cell dimensions	
a, *b*, *c* (Å)	76.5, 96.1, 101.2
$\alpha = \beta = \gamma$ (deg)	90
resolution (Å)	50.0−2.10
no. reflections observed	325,430
no. unique reflections	44,111
R_{merge} (%)[b]	13.5 (64.5)[a]
$I/\sigma I$	14.1 (3.2)[a]
% completeness	99.7 (96.5)[a]
Refinement	
resolution range	50−2.10
no. reflections in working set	44,070
no. reflections in test set	1,989
R_{work} (%)[c]	17.6 (22.0)
R_{free} (%)[c]	22.8 (29.4)
RMS deviation:	
bond lengths (Å)	0.01
bond angles (deg)	1.0
protein/water atoms	4247/342
average B-factors (Å^2)	
total	20.6
protein	20.2
water	24.9
ions	18.9
citrate	25.4

[a]The last resolution shell is shown in parentheses. [b]$R_{merge} = \Sigma_h\Sigma_I|I_I(h) - \langle I(h)\rangle|/\Sigma_h\Sigma_I I_I(h)$, where $I_I(h)$ is the i^{th} measurement and $\langle I(h)\rangle$ is the weighted mean of all measurements of $I(h)$. [c]R_{work} and $R_{free} = h(|F(h)_{obs}| - |F(h)_{calc}|)/h|F(h)_{obs}|$ for reflections in the working and test sets, respectively. RMS, root-mean-square.

RESULTS

Determination of SaFBA Crystal Structure. To understand more clearly how structural features, such as the Z-loop in SaFBA compare to other class II FBAs, SaFBA was expressed, purified, and screened against several suites of commercially available precipitant screens followed by optimization via an additive screen. The final crystal condition was comprised of 1.6 M ammonium citrate pH 7.5 and was optimized with 3 M NDSB 195, yielding a 2.1 Å data set in a $P2_12_12$ space group (Table 1).

SaFBA was observed as a dimer in the asymmetric unit with the secondary structure of each monomer resembling the TIM barrel fold of other class II FBAs, such as MtFBA (Figure 2a,b). The dimeric nature of SaFBA in the asymmetric unit is consistent with the oligomeric state suggested by size exclusion chromatography (data not shown). Of the SaFBA's 295 amino acids, all showed good electron density except for residues 1, 144, 145, 183−187, and 288−295. The structure is comprised of 12 α-helices and 8 β-sheets. Comparison of SaFBA and MtFBA immediately highlighted the differences between class IIb and class IIa FBAs. Several helices such as α3, α5, and α6 are shifted considerably, and helices α8b, α8c, and a 3_{10} in MtFBA are not present in SaFBA (Figure 2c). This is reflective of the additional length that class IIa FBAs possess over their class IIb counterparts.

Conversely, evaluation of SaFBA to the class IIb FBA from *Helicobacter pylori* (HpFBA) illustrates a higher degree of commonality. However, some noticeable differences are still present, particularly in relation to the β5α5 and β6α6 loops (Figure 2d). The β5α5 loop consisting of SaFBA residues 139−148, termed the active site loop as it contains a residue critical for the deprotonation/protonation step of the class II FBA-facilitated reaction, is highly flexible in the apo and holo forms of class II FBAs as evidenced by almost all elucidated class II FBA structures missing electron density of at least one, or more, residues within this region.[20,42,55] Likewise, in the active site loop of our SaFBA structure only residues Glu144 and Gln145 are missing.

Unlike the active site loop within class II FBAs, the β6α6 loop containing residues 177−191, and previously termed the Z-loop, is almost always well-defined structurally.[17,19,20,34,42,44,45,49,56−60] This loop forms part of the substrate pocket as well as contains a histidine residue involved in coordination with the active site Zn(II) ion.[46] Between class IIb FBAs, such as HpFBA, whose structures have been reported, and SaFBA, HpFBA possess two additional residues within this region. Additionally, all previously reported class IIb FBAs also possess an α-helix located near the Z-loop not seen in either SaFBA or MtFBA (Figure 2d). It is unclear whether this helix is influential in the enzyme's functionality, but it may

dx.doi.org/10.1021/bi501141t | *Biochemistry* 2014, 53, 7604−7614

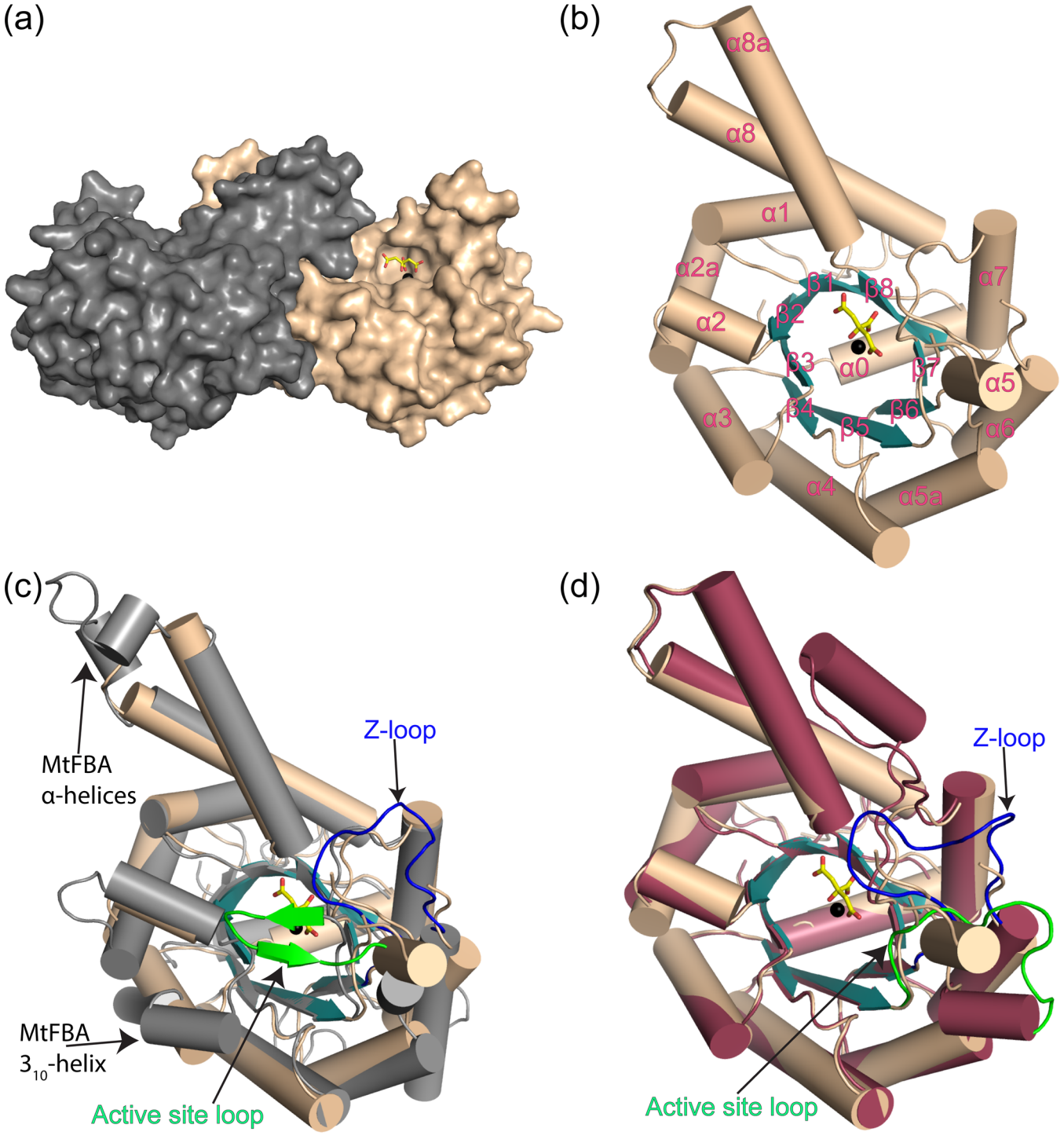

Figure 2. Secondary structure comparisons of Class II FBAs. (a) Surface rendering of the SaFBA dimer found in the asymmetric unit with one protomer colored tan, the other colored gray, citrate is shown as sticks and colored yellow, and Zn(II) ion is shown as a black sphere. (b) Cartoon rendering of the SaFBA protomer. Helical regions are represented as cylinders with β-strands as arrows. Helices and loops are colored tan with β-strands colored teal, citrate and Zn(II) are as in (a). (c) SaFBA the same as in (b) but overlaid with MtFBA-PGH (PDB code: 4DEL) shown in gray. The $\beta5\alpha5$ loop (green) and the $\beta6\alpha6$ loop (blue) for which is density is observed in the MtFBA-PGH structure but only partially in the SaFBA structure. (d) SaFBA same as in (b) but overlaid with HpFBA-TD4 (PDB code: 3N9S_A) shown in maroon. The $\beta5\alpha5$ loop (green) and the $\beta6\alpha6$ loop (blue) for which is density was observed in the HpFBA-TD4 structure and only partially in the SaFBA structure.

be part of the reason as to why HpFBA's Z-loop is two residues longer than that of SaFBA. Interestingly for the SaFBA structure, there was no electron density observed for residues 183−187 in its Z-loop, and His181 was displaced from its coordination of the Zn(II) ion. Closer inspection of this region using a simulated omit map revealed F_o-F_c density of a citrate molecule coordinating the active site Zn(II) in a tridentate manner (Figure 3). This interaction is curiously similar to that observed previously between MtFBA and the Z-loop inhibitor HCA. Naturally, the likely source of this citrate ion is the crystallization condition that contained 1.6 M ammonium citrate. Along with the three coordinating bonds to the citrate

dx.doi.org/10.1021/bi501141t | *Biochemistry* 2014, 53, 7604−7614

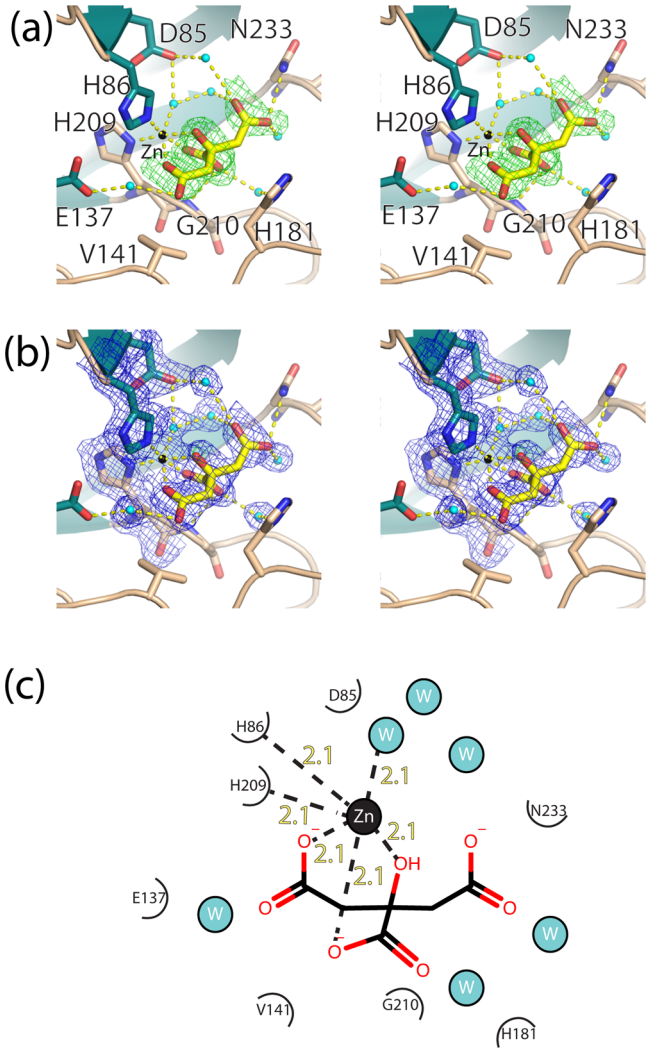

Figure 3. SaFBA active site. (a) Wall-eyed stereoview close-up of citrate (yellow) interacting with SaFBA (tan/teal), Zn(II) (black sphere), and waters (cyan spheres). Green mesh represents the F_o-F_c density from an simulated annealing omit scaled to 3σ when refined without the presence of citrate, black labels indicate SaFBA residues, and yellow dashed lines indicate distances no greater than 3.5 Å. (b) Same as in (a) except blue mesh represents final simulated annealing $2F_o-F_c$ map of citrate and adjacent residues scaled to 1σ and green mesh represents final simulated annealing F_o-F_c map scaled to 3σ. (c) Two-dimensional representation of citrate bound to SaFBA. Residues labels and crescents illustrate interactions of residues mediated through side chains with citrate, Zn(II) and surrounding waters within a 3.5 Å radius of citrate. For clarity, distances for only coordinating Zn(II) bonds are labeled yellow in angstroms.

ion, the active site Zn(II) also forms an additional three coordinating bonds with residues His86 and His209 and a water molecule. These interactions yield a coordination number of 6 (T_6) for the active site Zn(II) similar to that of the FBP-bound structure of MtFBA and different from the T_5 coordination found in the inhibitor-bound structure of HpFBA for which the entire protein was observed including the active site loop (Figure 4).[17,43] This coordination state is also different from the T_5 coordination state observed in the HCA bound MtFBA structure. Additionally, the citrate ion forms hydrogen bonds (H-bonds) with Asn233 and Gly210, as well as a network of H-bonds through several waters to Glu137, His181, and Asp85 (Figure 3).

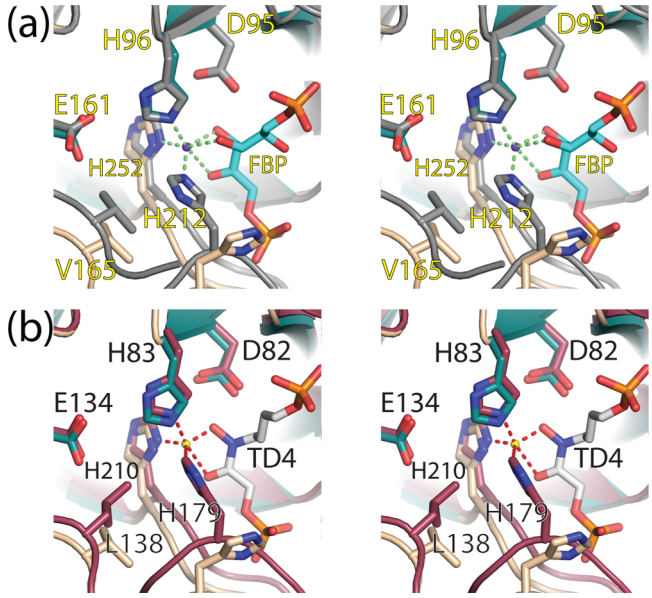

Figure 4. FBA active site comparison. (a) Wall-eyed stereoview of SaFBA (tan/teal) overlaid with MtFBA (gray; PDB entry 3ELF_A) interacting with FBP (cyan) and Zn(II) (purple) with green dashed lines indicating coordinating bonds. Yellow labels indicate MtFBA residues. (b) Wall-eyed stereoview of SaFBA colored as in (a) overlaid with HpFBA (lavender; PDB code: 3N9S_A) interacting with TD4 (white) and Zn(II) (yellow) with red dashed lines indicating coordinating bonds. Black labels indicate HpFBA residues.

Probing SaFBA's Substrate Affinity for FBP, HCA, and Citrate. FBAs catalyze the reversible aldol condensation of DHAP with G3P to form FBP. To gain insight on the affinity of SaFBA for FBP, a fluorescence-based assay was employed. Using the initial slopes over a series of FBP concentrations, the K_M and k_{cat} values of SaFBA for FBP were found to be 239 ± 16 μM and 69.5 ± 1.6 min^{-1}, respectively (Figure 5a). These values fall within the range of several other class II FBAs.[61−64]

Previously, we illustrated that HCA inhibited SaFBA activity; however, this data was obtained at a concentration of FBP over 3-fold lower than its K_M.[46] Therefore, to gain a more complete analysis of HCA's inhibition of SaFBA a dose−response relationship was conducted using a total of five different concentrations of FBP and ten different HCA concentrations. This allowed for determination of the mode of inhibition of HCA for SaFBA as well as to clarify whether that mode would be consistent with the noncompetitive manner observed when HCA inhibited MtFBA (Figure 5b). Surprisingly, unlike MtFBA whose k_{cat} changed while its K_M remained constant, both the k_{cat} as well as the K_M values of SaFBA varied for each condition tested. This along with nonlinear regression analysis indicated that HCA inhibits in a mixed manner with a K_i of 96 ± 22 μM (Figure 5b).

With a citrate ion located in the active site coordinating with the active site Zn(II) ion in a similar manner as that of HCA in the MtFBA-HCA structure, the ability of citrate to inhibit SaFBA was also explored.[46] Analyzing the dose−response inhibitory effects of citrate ion on SaFBA, while at the K_M of FBP, revealed an IC_{50} of 56.9 ± 3.5 mM with an I_{max} of 76.9 ± 1.9% (Figure 5d). This was 250-fold higher than that observed for HCA, IC_{50} of 227 ± 29 μM, at the same concentration (Figure 5c). Interestingly, previous studies on bacteria have proposed a citrate concentration within the cytoplasm in the range of 7−21 mM.[14,65] At the higher end of this range, SaFBA

dx.doi.org/10.1021/bi501141t | Biochemistry 2014, 53, 7604−7614

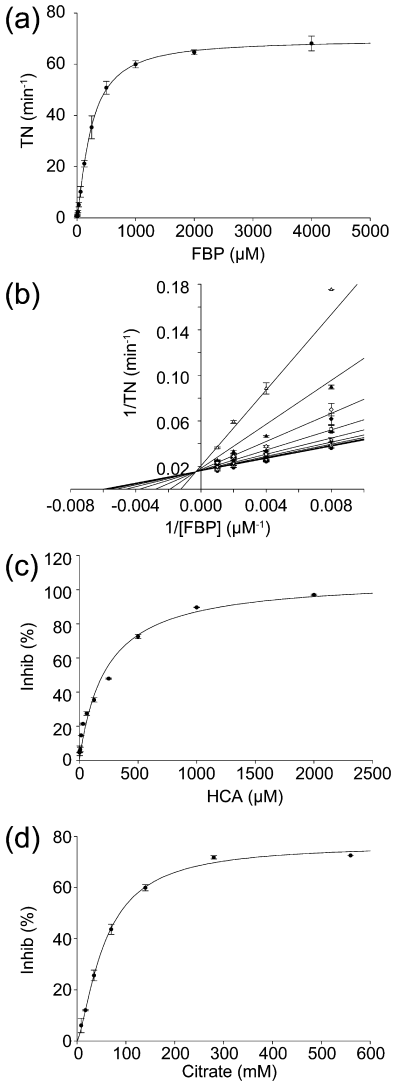

Figure 5. SaFBA kinetic studies. (a) Plot of turnover number (TN) of FBP by SaFBA as the concentration of FBP was varied from 0 to 5000 μM. (b) Lineweaver–Burke plot of inhibition of SaFBA by HCA. Concentrations of HCA were (●) 0, (○) 1.95, (▼) 3.91, (▽) 7.81, (■) 15.6, (□) 31.3, (♦) 62.5, (◊) 125, (▲) 250, and (△) 500 μM. Data were fit globally to a pure mixed inhibition model. (c) Plot of inhibition of SaFBA as the HCA concentration was increased from 0 to 2 mM. (d) Plot of inhibition of SaFBA as the citrate concentration was increased from 0 to 560 mM. All plots were fit to the Michaelis–Menten equation.

might be inhibited ~10%, or more, pending mode of inhibition. This suggests inhibition of SaFBA by citrate may warrant future studies to flesh out its biological significance.

DISCUSSION

Structural Based Categorization of Class II FBAs. Previously, class II FBAs could be grouped into either IIa or IIb on the basis of their sequence homology and oligomeric state.[19,20,39,40,64] Genetic studies of several pathogenic bacteria in which the *fba* gene was removed resulted in a loss of viability for the organism.[22−31] As a result, over the past few years the potential benefit of using class II FBAs as targets for therapeutic development has spurred the elucidation of a number of class II FBA structures.[17,19,20,34,42,45,66] Taking this additional structural information into consideration, the differences within these classes become readily apparent. For instance among class IIa FBAs, MtFBA possesses several helices facilitating a tetrameric organization setting itself structurally apart from all other structurally characterized class IIa FBAs, such as the one from *E. coli* as well as a recent unreported protein data bank entry from *Campylobacter jejuni* (PDB Code: 3QM3).[17] However, MtFBA is likely not alone in its tetrameric organization. Other class IIa FBAs, such as *Mycobacterium leprae* and *Coryenbacterium glutamicum*, may contain similar structural elements whose purpose in light of the MtFBA structure can now be realized.[41] Naturally, with the additional structural insight the MtFBA structure provided, a case can be made for two subtypes of class IIa, class IIai and class IIaii.

Similar to MtFBA, the SaFBA structure appears to have the same clarifying effect for class IIb FBAs. Previously, Plaumann et al. proposed possible functional roles to delineate class IIb FBA subtypes, while Henze et al. further outlined at least four class IIb FBA subtypes (i-iv).[40,41] Due to the limited data at the time neither group could definitively assemble each putative class IIb FBA studied into an appropriate subtype. Regrettably, subsequent reported structures of class IIb FBA structures from *H. pylori* and *Giardia lamblia* (GlFBA) provided only a little additional clarity. Although their sequence alignment score as determined by ClustalW was 0.41, analysis of the structures by the Proteins, Interfaces, Structures and Assemblies (PISA) server revealed a score of 0.80 indicating that they likely belong to a single subtype.[41,67] Intriguingly, when SaFBA was run through the PISA server it was shown to be most similar to the FBA from *Bacillus anthracis* (BaFBA) with a score of 0.88 and when compared to GlFBA both SaFBA and BaFBA scored roughly 0.70 implying that SaFBA and BaFBA likely fall into their own subtype. Using SaFBA along with the recent deposition of class IIb FBAs from *B. anthracis* (PDB Code: 3Q94) and *Coccoidioides immitis* (PDB Code: 3PM6) into the PDB, an updated categorization of class IIb subtypes can be envisioned (Figure 6).[42] Specifically, the class II FBAs from *G. lamblia* and *H. pylori* contain an insertion of ~21 residues that does not align with SaFBA or other class IIb FBAs such as BaFBA (Figure 1). The result of this insert is an additional α-helix seen in several class IIb FBAs but missing in others (Figure 6). The additional helix seen in the likes of GlFBA and HpFBA confirm the assertion by Henze et al. that they belong to the same subtype, class IIb-i. Although neither SaFBA nor BaFBA were previously analyzed for a class IIb subtype, both share >79% similarity and >80% identity with *Bacillus subtilis* which was categorized as class IIb-iv.[41] Furthermore, the nearly completely conserved crystal structures of SaFBA and the currently unreported BaFBA implicate that they belong to the same subtype. It remains to be determined structurally whether other subtypes exist as previously reported or what, if any, the functional differences between each subtype may be.[40,41] Therefore, SaFBA can most accurately be classified as a class IIb-iv. It is interesting to note that the additional helix in class IIb-i FBAs is positioned very near the Z-loop, and the composition of this helix may play a role in substrate binding. In the case of GlFBA, a shift in this loop was noticed when comparing the unbound structure to that of GlFBA with FBP bound.[44] Only with further mutagenesis and enzymatic testing will reveal the function and significance of this discrepancy between class IIb FBAs be elucidated.

Z-Loop Based Inhibitors. Previously, HCA was revealed to be a potential inhibitor for class IIa FBAs.[46] Specifically, several structures of MtFBA demonstrated the concept that

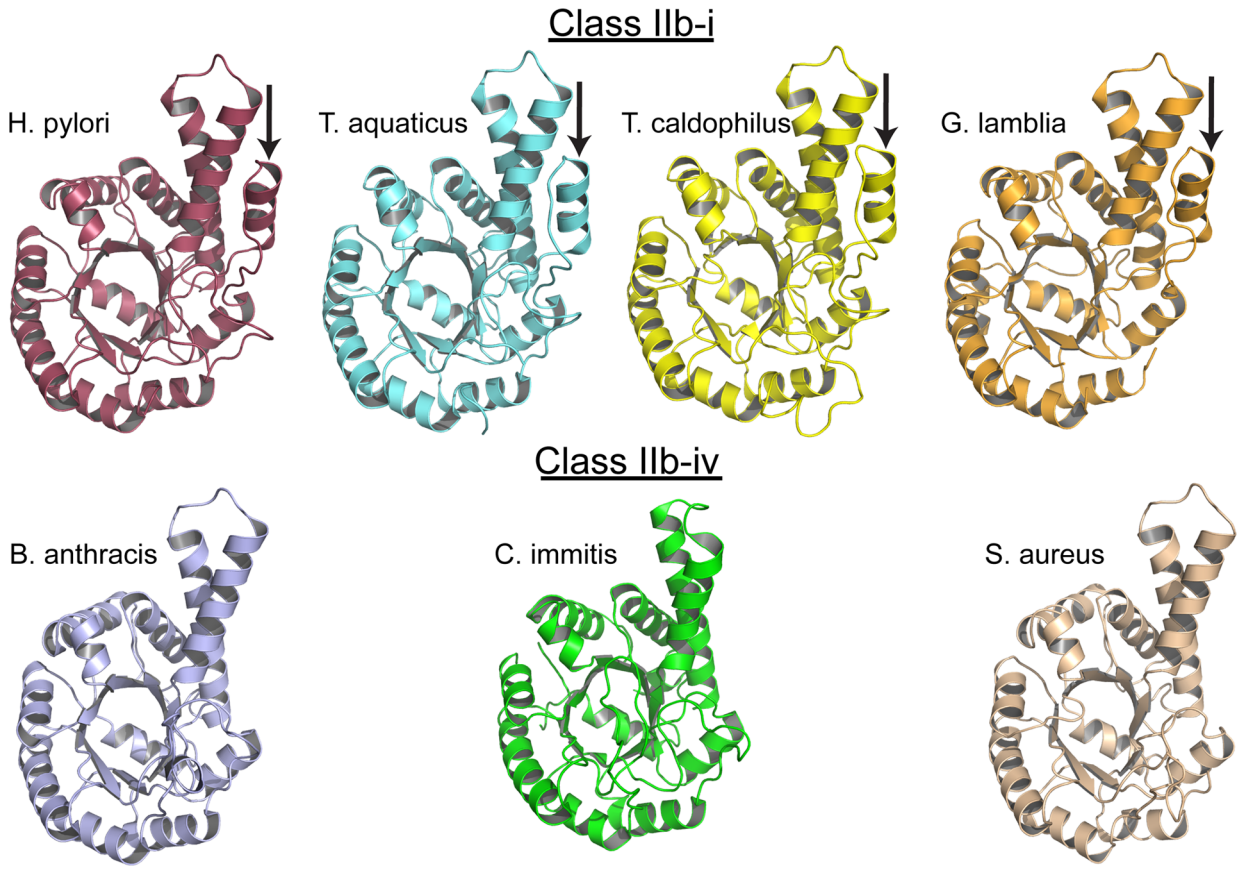

Figure 6. Structural comparison of class IIb FBA subtypes. (Top) Cartoon representations of the crystal structures for class IIb-i FBAs from *H. pylori* (PDB Code: 3N9S_A), *G. lamblia* (3GAK_B), *T. aquaticus* (1RV8_A), and *T. caldophilus* (2FJK_A). (Bottom) Cartoon representations of the crystal structures for class IIb-iv FBAs from *B. anthracis* (3Q94_A), *C. immitis* (3PM6_A), and *S. aureus* (PDB code: 4TO8_A). Arrows point to the loop and α helix seen in class IIb-i FBAs due to the 21 amino acid insertion.

HCA capitalized on the flexible dynamic nature of the Z-loop to create a hydrophobic pocket to bind. Based on both class IIa and IIb FBAs relying on an active site Zn(II) ion for enzymatic function, not surprisingly the identity of residues that comprise their active sites remain largely conserved (Figure 4). This includes those located in the Z-loop involved with coordination of the active site Zn(II). However, as previously discussed, the Z-loop itself is not entirely conserved between class IIa and class IIb FBAs, nor are many of the structural features surrounding it (Figures 1 and 2). Naturally, this spurred speculation whether the dynamic range observed in the Z-loop of MtFBA and the ability of HCA to capitalize on this feature is an isolated example, representative of only class IIa FBAs, or of class II FBAs in general. Fascinatingly, the SaFBA structure proposes the latter. Specifically, the SaFBA structure disclosed the ability of the small molecule citrate to wedge itself between the Z-loop of SaFBA and its Zn(II) in a related manner to that observed between MtFBA and HCA. Hence, demonstrating that even class IIb FBAs can be vulnerable to small molecules such as HCA, or other small molecules derived from that platform, which are designed to exploit the dynamic nature of the Z-loop (Figure 3).

Interestingly, while HCA inhibited the class IIa FBA from *M. tuberculosis* in a noncompetitive manner, the data from this study shows that HCA inhibits the class IIb FBA from *S. aureus* in a mixed fashion and with an almost 8-fold weaker K_i. Since class II FBAs all function via an active site Zn(II) ion, the reason for the different modes of inhibition may be more closely tied to the structural differences between the two subclasses. Structures of class IIb FBAs from *G. lamblia* and *B. anthracis* have been solved with FBP and DHAP bound respectively and illustrate that they bind in an identical fashion to that of MtFBA.[17,44] One of the major differences between class IIa and IIb FBAs is that class IIa possesses an active site loop which is ∼5 residues longer. As a result of this longer active site loop, HCA binding is not influenced by a substrate being present. Conversely, the presence of a substrate in a class IIb FBA would cause the hydrophobic pocket that HCA takes advantage of to be constricted due to the reduced length of the active site loop. As a result, for class IIb FBAs the presence of HCA likely reduces the ability for the active site loop to interact with the substrates. The fact that HCA appears to bind more tightly to MtFBA than SaFBA, as indicted by their differences in K_i, suggests that the longer active site loop aids in HCA binding. Since the active site loop does not appear to form any direct interactions with HCA in MtFBA, it is likely that the reduced strain on the hydrophobic pocket of the binding site is responsible for the increase in binding. Of course more data will be necessary to verify these conclusions such as determining HCA's mode of action against other class IIa/b FBAs as well as obtaining a crystal structure of a class IIb FBA with HCA bound. However, the fact that the mobility of the Z-loop allows for the incorporation of small molecules, such as HCA and citrate, that capitalize on the coordination of the active site Zn(II) ion, as well as the active site residue, adds to

dx.doi.org/10.1021/bi501141t | *Biochemistry* 2014, 53, 7604−7614

the structural information on class II FBAs which can be utilized to design potential inhibitors.

■ ASSOCIATED CONTENT

Accession Codes

The atomic coordinates and structure factors have been deposited with the Brookhaven Protein Data Bank (PDB codes 4TO8).

■ AUTHOR INFORMATION

Corresponding Author

*Phone: 706 542 3435. E-mail: spegan@uga.edu. Corresponding author address: College of Pharmacy, University of Georgia, 422 Pharmacy South, Athens, GA 30602.

Funding

This research was supported in part by grants from the Colorado Center for Drug Discovery, Cancer Center Support Grant P30CA046934, and the National Institutes of Health Grants 1R01Al109008-01 (SDP). The Advanced Light Source is supported by the Director, Office of Science, Office of Basic Energy Sciences, of the U.S. Department of Energy under Contract No. DE-AC02-05CH11231.

Notes

The authors declare the following competing financial interest(s): A provisional U.S. Patent Application No. 61/821,184 and U.S. Patent Application No. 14/273,411 have been filed.

■ ABBREVIATIONS:

ALS, Advanced Light Source; BaFBA, *Bacillus anthracis* class II fructose 1,6-bisphosphate aldolase; BSA, bovine serum albumin; CA, Community Acquired; CDC, Centers for Disease Control; DHAP, dihydroxyacetone phosphate; DMSO, dimethyl sulfoxide; DTT, dithiothreitol; FBP, fructose 1,6-bisphosphate; GAPDH, glyceraldehyde 3-phosphate dehydrogenase; GlFBA, *Giardia lamblia* class II fructose 1,6-bisphosphate aldolase; G3P, glyceraldehyde 3-phosphate; H-bond, hydrogen bond; HpFBA, *Helicobacter pyloria* class II fructose 1,6-bisphosphate aldolase; HA, Hospital-Acquired; HACO, Healthcare-Associated Community-Onset; HCA, 8-hydroxyquinoline-2-carboxylic acid; HEPES, *N*-(2-hydroxyethyl)piperazine-*N*′-2-ethanesulfonate; IPTG, isopropyl *β*-D-thiogalactoside; LB, Luria−Bertani; MRSA, methicillin-resistant *Staphylococcus aureus*; MtFBA, *Mycobacterium tuberculosis* class II fructose 1,6-bisphosphate aldolase; NAD^+, nicotinamide adenine dinucleotide; NADH, reduced nicotinamide adenine dinucleotide; Ni-NTA, nickel nitrilotriacetic acid; PBP, penicillin-binding Protein; PDB, Protein Data Bank; PEG, polyethylene glycol; PGH, phosphoglycolohydroxamate; SaFBA, *Staphylococcus aureus* class II fructose 1,6-bisphosphate aldolase; SDS−PAGE, sodium dodecyl sulfate polyacrylamide gel electrophoresis; TD4, 4-[hydroxy[(phosphonooxy)acetyl]-amino]butyl dihydrogen phosphate; TPI, triosephosphate isomerase; TN, Turnover Number; Z-loop, zinc-binding loop

■ REFERENCES

(1) Pottinger, P. S. (2013) Methicillin-resistant Staphylococcus aureus infections. *Med. Clin. North Am. 97*, 601−619.

(2) Casey, J. A., Curriero, F. C., Cosgrove, S. E., Nachman, K. E., and Schwartz, B. S. (2013) High-density livestock operations, crop field application of manure, and risk of community-associated methicillin-resistant Staphylococcus aureus infection in Pennsylvania. *JAMA Intern. Med. 173*, 1980−1990.

(3) Centers for Disease Control and Prevention. *Active Bacterial Core Surveillance (ABCs) Report Emerging Infections Program Network Methicillin-Resistant Staphylococcus aureus, 2011*; 2011.

(4) Dantes, R., Mu, Y., Belflower, R., Aragon, D., Dumyati, G., Harrison, L. H., Lessa, F. C., Lynfield, R., Nadle, J., Petit, S., Ray, S. M., Schaffner, W., Townes, J., Fridkin, S., and Emerging Infections Program-Active Bacterial Core Surveillance MRSA Surveillance Investigators. (2013) National burden of invasive methicillin-resistant Staphylococcus aureus infections, United States, 2011. *JAMA Intern. Med. 173*, 1970−1978.

(5) Hunt, C., Dionne, M., Delorme, M., Murdock, D., Erdrich, A., Wotsey, D., Groom, A., Cheek, J., Jacobson, J., Cunningham, B., Shirley, L., Belai, K., Kurachek, S., Ackerman, P., Cameron, S., Schlievert, P., Pfeiffer, J., Johnson, S., Boxrud, D., Bartkus, J., Besser, J., Smith, K., LeDell, K., O'Boyle, C., Lynfield, R., White, K., Osterholm, M., Moore, K., Danilla, R., and Cdc (1999) Four pediatric deaths from community-acquired methicillin-resistant Staphylococcus aureus - Minnesota and North Dakota, 1997−1999 (Reprinted from MMWR). *Arch. Dermatol. 135*, 1566−1568.

(6) Klevens, R. M., Edwards, J. R., Tenover, F. C., McDonald, L. C., Horan, T., Gaynes, R., and National Nosocomial Infections Surveillance System. (2006) Changes in the epidemiology of methicillin-resistant Staphylococcus aureus in intensive care units in US hospitals, 1992−2003. *Clin. Infect. Dis. 42*, 389−391.

(7) Baquero, F. (1997) Gram-positive resistance: challenge for the development of new antibiotics. *J. Antimicrob. Chemother. 39* (Suppl A), 1−6.

(8) Bauernfeind, A., Thornsberry, C., Grassi, G. G., Painter, B. G., Peters, G., Shlaes, D. M., and Stratton, C. W. (1994) Quinolone Resistance in Gram-Positive Bacteria - Panel Discussion. *Infect. Dis. Clin. Pract. 3*, S133−S135.

(9) Crossley, K., Loesch, D., Landesman, B., Mead, K., Chern, M., and Strate, R. (1979) An outbreak of infections caused by strains of Staphylococcus aureus resistant to methicillin and aminoglycosides. I. Clinical studies. *J. Infect. Dis. 139*, 273−279.

(10) Kaufhold, A., Behrendt, W., Krauss, T., and van Saene, H. (1992) Selective decontamination of the digestive tract and methicillin-resistant Staphylococcus aureus. *Lancet 339*, 1411−1412.

(11) Mainardi, J. L., Shlaes, D. M., Goering, R. V., Shlaes, J. H., Acar, J. F., and Goldstein, F. W. (1995) Decreased teicoplanin susceptibility of methicillin-resistant strains of Staphylococcus aureus. *J. Infect. Dis. 171*, 1646−1650.

(12) Schwalbe, R. S., Stapleton, J. T., and Gilligan, P. H. (1987) Emergence of vancomycin resistance in coagulase-negative staphylococci. *N. Engl. J. Med. 316*, 927−931.

(13) Shlaes, D. M., and Shlaes, J. H. (1995) Teicoplanin selects for Staphylococcus aureus that is resistant to vancomycin. *Clin. Infect. Dis. 20*, 1071−1073.

(14) Barrett, F. F., McGehee, R. F., Jr., and Finland, M. (1968) Methicillin-resistant Staphylococcus aureus at Boston City Hospital. Bacteriologic and epidemiologic observations. *N. Engl. J. Med. 279*, 441−448.

(15) Rutter, W. J. (1964) Evolution of Aldolase. *Fed. Proc. 23*, 1248−1257.

(16) Lorentzen, E., Siebers, B., Hensel, R., and Pohl, E. (2005) Mechanism of the Schiff base forming fructose-1,6-bisphosphate aldolase: structural analysis of reaction intermediates. *Biochemistry 44*, 4222−4229.

(17) Pegan, S. D., Rukseree, K., Franzblau, S. G., and Mesecar, A. D. (2009) Structural basis for catalysis of a tetrameric class IIa fructose 1,6-bisphosphate aldolase from Mycobacterium tuberculosis. *J. Mol. Biol. 386*, 1038−1053.

(18) Zgiby, S., Plater, A. R., Bates, M. A., Thomson, G. J., and Berry, A. (2002) A functional role for a flexible loop containing Glu182 in the class II fructose-1,6-bisphosphate aldolase from Escherichia coli. *J. Mol. Biol. 315*, 131−140.

(19) Galkin, A., Kulakova, L., Melamud, E., Li, L., Wu, C., Mariano, P., Dunaway-Mariano, D., Nash, T. E., and Herzberg, O. (2007) Characterization, kinetics, and crystal structures of fructose-1,6-

bisphosphate aldolase from the human parasite, Giardia lamblia. *J. Biol. Chem. 282*, 4859−4867.
(20) Izard, T., and Sygusch, J. (2004) Induced fit movements and metal cofactor selectivity of class II aldolases: structure of Thermus aquaticus fructose-1,6-bisphosphate aldolase. *J. Biol. Chem. 279*, 11825−11833.
(21) Marsh, J. J., and Lebherz, H. G. (1992) Fructose-bisphosphate aldolases: an evolutionary history. *Trends Biochem. Sci. 17*, 110−113.
(22) Baba, T., Ara, T., Hasegawa, M., Takai, Y., Okumura, Y., Baba, M., Datsenko, K. A., Tomita, M., Wanner, B. L., and Mori, H. (2006) Construction of Escherichia coli K-12 in-frame, single-gene knockout mutants: the Keio collection. *Mol. Syst. Biol. 2*, 2006 0008.
(23) Gerdes, S. Y., Scholle, M. D., Campbell, J. W., Balazsi, G., Ravasz, E., Daugherty, M. D., Somera, A. L., Kyrpides, N. C., Anderson, I., Gelfand, M. S., Bhattacharya, A., Kapatral, V., D'Souza, M., Baev, M. V., Grechkin, Y., Mseeh, F., Fonstein, M. Y., Overbeek, R., Barabasi, A. L., Oltvai, Z. N., and Osterman, A. L. (2003) Experimental determination and system level analysis of essential genes in Escherichia coli MG1655. *J. Bacteriol. 185*, 5673−5684.
(24) Giaever, G., Chu, A. M., Ni, L., Connelly, C., Riles, L., Veronneau, S., Dow, S., Lucau-Danila, A., Anderson, K., Andre, B., Arkin, A. P., Astromoff, A., El-Bakkoury, M., Bangham, R., Benito, R., Brachat, S., Campanaro, S., Curtiss, M., Davis, K., Deutschbauer, A., Entian, K. D., Flaherty, P., Foury, F., Garfinkel, D. J., Gerstein, M., Gotte, D., Guldener, U., Hegemann, J. H., Hempel, S., Herman, Z., Jaramillo, D. F., Kelly, D. E., Kelly, S. L., Kotter, P., LaBonte, D., Lamb, D. C., Lan, N., Liang, H., Liao, H., Liu, L., Luo, C., Lussier, M., Mao, R., Menard, P., Ooi, S. L., Revuelta, J. L., Roberts, C. J., Rose, M., Ross-Macdonald, P., Scherens, B., Schimmack, G., Shafer, B., Shoemaker, D. D., Sookhai-Mahadeo, S., Storms, R. K., Strathern, J. N., Valle, G., Voet, M., Volckaert, G., Wang, C. Y., Ward, T. R., Wilhelmy, J., Winzeler, E. A., Yang, Y., Yen, G., Youngman, E., Yu, K., Bussey, H., Boeke, J. D., Snyder, M., Philippsen, P., Davis, R. W., and Johnston, M. (2002) Functional profiling of the Saccharomyces cerevisiae genome. *Nature 418*, 387−391.
(25) Jacobs, M. A., Alwood, A., Thaipisuttikul, I., Spencer, D., Haugen, E., Ernst, S., Will, O., Kaul, R., Raymond, C., Levy, R., Chun-Rong, L., Guenthner, D., Bovee, D., Olson, M. V., and Manoil, C. (2003) Comprehensive transposon mutant library of Pseudomonas aeruginosa. *Proc. Natl. Acad. Sci. U.S.A. 100*, 14339−14344.
(26) Kobayashi, K., Ehrlich, S. D., Albertini, A., Amati, G., Andersen, K. K., Arnaud, M., Asai, K., Ashikaga, S., Aymerich, S., Bessieres, P., Boland, F., Brignell, S. C., Bron, S., Bunai, K., Chapuis, J., Christiansen, L. C., Danchin, A., Debarbouille, M., Dervyn, E., Deuerling, E., Devine, K., Devine, S. K., Dreesen, O., Errington, J., Fillinger, S., Foster, S. J., Fujita, Y., Galizzi, A., Gardan, R., Eschevins, C., Fukushima, T., Haga, K., Harwood, C. R., Hecker, M., Hosoya, D., Hullo, M. F., Kakeshita, H., Karamata, D., Kasahara, Y., Kawamura, F., Koga, K., Koski, P., Kuwana, R., Imamura, D., Ishimaru, M., Ishikawa, S., Ishio, I., Le Coq, D., Masson, A., Mauel, C., Meima, R., Mellado, R. P., Moir, A., Moriya, S., Nagakawa, E., Nanamiya, H., Nakai, S., Nygaard, P., Ogura, M., Ohanan, T., O'Reilly, M., O'Rourke, M., Pragai, Z., Pooley, H. M., Rapoport, G., Rawlins, J. P., Rivas, L. A., Rivolta, C., Sadaie, A., Sadaie, Y., Sarvas, M., Sato, T., Saxild, H. H., Scanlan, E., Schumann, W., Seegers, J. F., Sekiguchi, J., Sekowska, A., Seror, S. J., Simon, M., Stragier, P., Studer, R., Takamatsu, H., Tanaka, T., Takeuchi, M., Thomaides, H. B., Vagner, V., van Dijl, J. M., Watabe, K., Wipat, A., Yamamoto, H., Yamamoto, M., Yamamoto, Y., Yamane, K., Yata, K., Yoshida, K., Yoshikawa, H., Zuber, U., and Ogasawara, N. (2003) Essential Bacillus subtilis genes. *Proc. Natl. Acad. Sci. U.S.A. 100*, 4678−4683.
(27) Liberati, N. T., Urbach, J. M., Miyata, S., Lee, D. G., Drenkard, E., Wu, G., Villanueva, J., Wei, T., and Ausubel, F. M. (2006) An ordered, nonredundant library of Pseudomonas aeruginosa strain PA14 transposon insertion mutants. *Proc. Natl. Acad. Sci. U.S.A. 103*, 2833−2838.
(28) Rodaki, A., Young, T., and Brown, A. J. (2006) Effects of depleting the essential central metabolic enzyme fructose-1,6-bisphosphate aldolase on the growth and viability of Candida albicans: implications for antifungal drug target discovery. *Eukaryotic Cell 5*, 1371−1377.
(29) Sassetti, C. M., Boyd, D. H., and Rubin, E. J. (2003) Genes required for mycobacterial growth defined by high density mutagenesis. *Mol. Microbiol. 48*, 77−84.
(30) Song, J. H., Ko, K. S., Lee, J. Y., Baek, J. Y., Oh, W. S., Yoon, H. S., Jeong, J. Y., and Chun, J. (2005) Identification of essential genes in Streptococcus pneumoniae by allelic replacement mutagenesis. *Mol. Cells 19*, 365−374.
(31) Wehmeier, U. F. (2001) Molecular cloning, nucleotide sequence and structural analysis of the Streptomyces galbus DSM40480 fda gene: the S-galbus fructose-1,6-bisphosphate aldolase is a member of the class II aldolases. *FEMS Microbiol. Lett. 197*, 53−58.
(32) Scamuffa, M. D., and Caprioli, R. M. (1980) Comparison of the mechanisms of two distinct aldolases from Escherichia coli grown on gluconeogenic substrates. *Biochim. Biophys. Acta 614*, 583−590.
(33) Stribling, D., and Perham, R. N. (1973) Purification and characterization of two fructose diphosphate aldolases from Escherichia coli (Crookes' strain). *Biochem. J. 131*, 833−841.
(34) Fonvielle, M., Coincon, M., Daher, R., Desbenoit, N., Kosieradzka, K., Barilone, N., Gicquel, B., Sygusch, J., Jackson, M., and Therisod, M. (2008) Synthesis and biochemical evaluation of selective inhibitors of class II fructose bisphosphate aldolases: towards new synthetic antibiotics. *Chemistry 14*, 8521−8529.
(35) Fonvielle, M., Weber, P., Dabkowska, K., and Therisod, M. (2004) New highly selective inhibitors of class II fructose-1,6-bisphosphate aldolases. *Bioorg. Med. Chem. Lett. 14*, 2923−2926.
(36) Gavalda, S., Braga, R., Dax, C., Vigroux, A., and Blonski, C. (2005) N-Sulfonyl hydroxamate derivatives as inhibitors of class II fructose-1,6-diphosphate aldolase. *Bioorg. Med. Chem. Lett. 15*, 5375−5377.
(37) Labbe, G., Krismanich, A. P., de Groot, S., Rasmusson, T., Shang, M., Brown, M. D., Dmitrienko, G. I., and Guillemette, J. G. (2012) Development of metal-chelating inhibitors for the Class II fructose 1,6-bisphosphate (FBP) aldolase. *J. Inorg. Biochem. 112*, 49−58.
(38) Li, D., Han, X., Tu, Q., Feng, L., Wu, D., Sun, Y., Chen, H., Li, Y., Ren, Y., and Wan, J. (2013) Structure-Based Design and Synthesis of Novel Dual-Target Inhibitors against Cyanobacterial Fructose-1,6-Bisphosphate Aldolase and Fructose-1,6-Bisphosphatase. *J. Agric. Food Chem. 61*, 7453−7461.
(39) Nakahara, K., Yamamoto, H., Miyake, C., and Yokota, A. (2003) Purification and characterization of class-I and class-II fructose-1,6-bisphosphate aldolases from the cyanobacterium Synechocystis sp. PCC 6803. *Plant Cell Physiol. 44*, 326−333.
(40) Plaumann, M., Pelzer-Reith, B., Martin, W. F., and Schnarrenberger, C. (1997) Multiple recruitment of class-I aldolase to chloroplasts and eubacterial origin of eukaryotic class-II aldolases revealed by cDNAs from Euglena gracilis. *Curr. Genet 31*, 430−438.
(41) Henze, K., Morrison, H. G., Sogin, M. L., and Muller, M. (1998) Sequence and phylogenetic position of a class II aldolase gene in the amitochondriate protist, Giardia lamblia. *Gene 222*, 163−168.
(42) Abendroth, J., Gardberg, A. S., Robinson, J. I., Christensen, J. S., Staker, B. L., Myler, P. J., Stewart, L. J., and Edwards, T. E. (2011) SAD phasing using iodide ions in a high-throughput structural genomics environment. *J. Struct. Funct. Genomics 12*, 83−95.
(43) Daher, R., Coincon, M., Fonvielle, M., Gest, P. M., Guerin, M. E., Jackson, M., Sygusch, J., and Therisod, M. (2010) Rational design, synthesis, and evaluation of new selective inhibitors of microbial class II (zinc dependent) fructose bis-phosphate aldolases. *J. Med. Chem. 53*, 7836−7842.
(44) Galkin, A., Li, Z., Li, L., Kulakova, L., Pal, L. R., Dunaway-Mariano, D., and Herzberg, O. (2009) Structural insights into the substrate binding and stereoselectivity of giardia fructose-1,6-bisphosphate aldolase. *Biochemistry 48*, 3186−3196.
(45) Lee, J. H., Bae, J., Kim, D., Choi, Y., Im, Y. J., Koh, S., Kim, J. S., Kim, M. K., Kang, G. B., Hong, S. I., Lee, D. S., and Eom, S. H. (2006) Stereoselectivity of fructose-1,6-bisphosphate aldolase in Thermus caldophilus. *Biochem. Biophys. Res. Commun. 347*, 616−625.

(46) Capodagli, G. C., Sedhom, W. G., Jackson, M., Ahrendt, K. A., and Pegan, S. D. (2013) A Noncompetitive Inhibitor for Mycobacterium tuberculosis's Class IIa Fructose 1,6-Bisphosphate Aldolase. *Biochemistry 53*, 202−213.
(47) Collins, K. D. (1974) An activated intermediate analogue. The use of phosphoglycolohydroxamate as a stable analogue of a transiently occurring dihydroxyacetone phosphate-derived enolate in enzymatic catalysis. *J. Biol. Chem. 249*, 136−142.
(48) Dreyer, M. K., and Schulz, G. E. (1996) Catalytic mechanism of the metal-dependent fuculose aldolase from Escherichia coli as derived from the structure. *J. Mol. Biol. 259*, 458−466.
(49) Li, Z., Liu, Z., Cho, D. W., Zou, J., Gong, M., Breece, R. M., Galkin, A., Li, L., Zhao, H., Maestas, G. D., Tierney, D. L., Herzberg, O., Dunaway-Mariano, D., and Mariano, P. S. (2011) Rational design, synthesis and evaluation of first generation inhibitors of the Giardia lamblia fructose-1,6-biphosphate aldolase. *J. Inorg. Biochem. 105*, 509−517.
(50) Gill, S. C., and von Hippel, P. H. (1989) Calculation of protein extinction coefficients from amino acid sequence data. *Anal. Biochem. 182*, 319−326.
(51) Kabsch, W. (2010) Xds. *Acta Crystallogr., Sect. D: Biol. Crystallogr. 66*, 125−132.
(52) Bailey, S. (1994) The Ccp4 Suite - Programs for Protein Crystallography. *Acta Crystallogr., Sect. D: Biol. Crystallogr. 50*, 760−763.
(53) Adams, P. D., Afonine, P. V., Bunkoczi, G., Chen, V. B., Davis, I. W., Echols, N., Headd, J. J., Hung, L. W., Kapral, G. J., Grosse-Kunstleve, R. W., McCoy, A. J., Moriarty, N. W., Oeffner, R., Read, R. J., Richardson, D. C., Richardson, J. S., Terwilliger, T. C., and Zwart, P. H. (2010) PHENIX: a comprehensive Python-based system for macromolecular structure solution. *Acta Crystallogr., Sect. D: Biol. Crystallogr. 66*, 213−221.
(54) Emsley, P., and Cowtan, K. (2004) Coot: model-building tools for molecular graphics. *Acta Crystallogr., Sect. D: Biol. Crystallogr. 60*, 2126−2132.
(55) Blom, N. S., Tetreault, S., Coulombe, R., and Sygusch, J. (1996) Novel active site in Escherichia coli fructose 1,6-bisphosphate aldolase. *Nat. Struct. Biol. 3*, 856−862.
(56) Gardberg, A., Abendroth, J., Bhandari, J., Sankaran, B., and Staker, B. (2011) Structure of fructose bisphosphate aldolase from Bartonella henselae bound to fructose 1,6-bisphosphate. *Acta Crystallogr., Sect. F: Struct. Biol. Cryst. Commun. 67*, 1051−1054.
(57) Gardberg, A., Sankaran, B., Davies, D., Bhandari, J., Staker, B., and Stewart, L. (2011) Structure of fructose bisphosphate aldolase from Encephalitozoon cuniculi. *Acta Crystallogr., Sect. F: Struct. Biol. Cryst. Commun. 67*, 1055−1059.
(58) Hall, D. R., Leonard, G. A., Reed, C. D., Watt, C. I., Berry, A., and Hunter, W. N. (1999) The crystal structure of Escherichia coli class II fructose-1, 6-bisphosphate aldolase in complex with phosphoglycolohydroxamate reveals details of mechanism and specificity. *J. Mol. Biol. 287*, 383−394.
(59) Kim, H., Certa, U., Dobeli, H., Jakob, P., and Hol, W. G. (1998) Crystal structure of fructose-1,6-bisphosphate aldolase from the human malaria parasite Plasmodium falciparum. *Biochemistry 37*, 4388−4396.
(60) de la Paz Santangelo, M., Gest, P. M., Guerin, M. E., Coinçon, M., Pham, H., Ryan, G., Puckett, S. E., Spencer, J. S., Gonzalez-Juarrero, M., Daher, R., Lenaerts, A. J., Schnappinger, D., Therisod, M., Ehrt, S., Sygusch, J., and Jackson, M. (2011) Glycolytic and Non-glycolytic Functions of Mycobacterium tuberculosis Fructose-1,6-bisphosphate Aldolase, an Essential Enzyme Produced by Replicating and Non-replicating Bacilli. *J. Biol. Chem. 286*, 40219−40231.
(61) Hao, J., and Berry, A. (2004) A thermostable variant of fructose bisphosphate aldolase constructed by directed evolution also shows increased stability in organic solvents. *Protein Eng., Des. Sel. 17*, 689−697.
(62) Pelzer-Reith, B., Wiegand, S., and Schnarrenberger, C. (1994) Plastid Class I and Cytosol Class II Aldolase of Euglena gracilis (Purification and Characterization). *Plant Physiol. 106*, 1137−1144.
(63) Mabiala-Bassiloua, C. G., Zwolinska, M., Therisod, H., Sygusch, J., and Therisod, M. (2008) Separate synthesis and evaluation of glucitol bis-phosphate and mannitol bis-phosphate, as competitive inhibitors of fructose bis-phosphate aldolases. *Bioorg. Med. Chem. Lett. 18*, 1735−1737.
(64) Sauve, V., and Sygusch, J. (2001) Molecular cloning, expression, purification, and characterization of fructose-1,6-bisphosphate aldolase from Thermus aquaticus. *Protein Expression Purif. 21*, 293−302.
(65) Nurmohamed, S., Vincent, H. A., Titman, C. M., Chandran, V., Pears, M. R., Du, D. J., Griffin, J. L., Callaghan, A. J., and Luisi, B. F. (2011) Polynucleotide Phosphorylase Activity May Be Modulated by Metabolites in Escherichia coli. *J. Biol. Chem. 286*, 14315−14323.
(66) Cooper, S. J., Leonard, G. A., McSweeney, S. M., Thompson, A. W., Naismith, J. H., Qamar, S., Plater, A., Berry, A., and Hunter, W. N. (1996) The crystal structure of a class II fructose-1,6-bisphosphate aldolase shows a novel binuclear metal-binding active site embedded in a familiar fold. *Structure 4*, 1303−1315.
(67) Krissinel, E., and Henrick, K. (2007) Inference of macromolecular assemblies from crystalline state. *J. Mol. Biol. 372*, 774−797.